

## Feasibility and Uncertainties Associated with Two-Angle Imaging of Sprays: A Focus on 3D Velocity Measurements

P.X. Pham<sup>1</sup>, A. Kourmatzis<sup>2</sup> and A.R. Masri<sup>1</sup>

<sup>1</sup>School of Aerospace, Mechanical and Mechatronics Engineering,  
The University of Sydney, New South Wales 2006, Australia

<sup>2</sup>Department of Engineering, Macquarie University, New South Wales, 2109, Australia

### Abstract

Backlight imaging is a standard experimental technique used for the measurement of liquid fragment size and velocity in multiphase flows. When used with appropriate microscope lenses, quantitative information on the spray structure can be attained, including measurement of non-spherical objects. A critical issue resides in the nature of the measurement which is line integrated from a single viewing angle. This fundamental limitation makes it impossible to resolve three dimensional information from the images. This paper presents the use of a pair of high speed cameras and long working distance microscopes oriented at 90 degrees to each-other, and synchronized to two high speed diode lasers. By assuming a particular fragment consists of multiple three-dimensional ellipsoids, an approximate fragment volume and velocity can be derived. Mono-dispersed drops generated by different syringe sizes along with micro-polyspheres are used as calibration tools to examine the feasibility of combined volume and velocity measurement from two viewing angles. The results reported in this work focus on velocity measurements which yield an uncertainty of up to 15% when compared to theory.

### Introduction

Our understanding of turbulent spray combustion, which is relevant to common practical devices including IC engines and boilers is limited due to the complexity of physical and chemical processes which are governed by short timescales and are a function of pressure and temperature variations. One of the most important physical processes is atomization where the bulk liquid breaks up to form different fragment sizes and shapes close to nozzle exit (primary breakup) [1-2]. The fragments, which move at a relative velocity to the surrounding environment deform and breakup into smaller drops and other fragments due to aerodynamic forces (secondary breakup) [3-5].

Early developments of IC engines have relied heavily on cut-and-try methods and empirical correlations using macro-information of the spray such as liquid spray penetration, spray cone angle, and droplet size distributions [6]. Practical spray jets, however, are initially dictated by instabilities (Rayleigh-Taylor and Kelvin-Helmoltz) to form ligaments and elongated/irregular shapes which cannot be accurately detected by conventional light scattering techniques. As such, developing experimental methods to visualize and quantify three dimensional, non-spherical objects is imperative. Details of irregular shapes are also relevant and critically important towards utilization of highly viscous fuels such as biodiesels with long carbon chain length and/or high saturation degree [7-8].

This work aims to extend previous backlit 2D-imaging techniques [9-10] to visualize 3D irregular shapes and quantify their dimensions and velocity using a pair of high-speed cameras equipped with microscopes and synchronised to two high-speed lasers. In the frame of this contribution, only velocity estimation is

reported. As an extension to this approach, the feasibility of quantification of fragment volume has also been tested successfully and this will be reported in a separate article. Firstly we present the experiment setup and code development, followed by results and discussion which include extensive calibration steps.

### Experiment Description

The experimental layout is an extension of a one-dimensional backlight illumination system to include two lasers, two lenses and two cameras both operated in a PIV mode and synchronized to the lasers using a LaVISION high-speed controller. Figure 1 shows a schematic of the experimental setup. Two x 5 kHz Edgewave laser heads (items 1&2 shown in Figure 1) are used in order to provide 2x532nm beams. Each beam is split into two beams oriented 90 degrees to each other using a 50-50 non-polarized beam-splitter (items 9&10 shown in Figure 1). Each pair of the four split beams is then delivered into two diffusing optics (7&8) and into the measurement volume. On the collection side of each viewing angle, there is a QM100 long-distance microscope (5&6) coupled to a LaVISION HSS6 camera (3&4). The distance between the diffusing optics and the measurement volume as well as the distance between the measurement volume and the front of the microscope lens is kept fixed for both viewing angles, to within an accuracy of 1mm, where further adjustments are made from the microscope in order to assure identical fields of view between two cameras. In these experiments, the spatial resolution for both cameras is fixed at 3.24  $\mu\text{m}/\text{pixel}$  with a field of view of 2.49 mm. One camera, under PIV mode, is operated under double exposure at two different times  $t_0$  and  $t_1$ , respectively. Therefore, the two cameras record a total of four 2D frames.

A technique based on the summation of ellipsoids has recently been developed by the same authors to quantify volume of liquid fragments by discretising them into a number of constituent ellipsoids [11]. This technique was initially tested against shapes of a known volume, and subsequently applied to a real spray. When correcting for fragment orientation using information from both lenses, measurements of volume using this new two-angle image processing methodology results in errors of no more than 10%. This work extends the technique to include a capability of quantifying velocity along with volume measurements.

To calibrate the velocity and volume measuring technique, different particle types are used including both paramagnetic polyethylene microspheres and mono-dispersed liquid drops. Four types of solid particles used in this tests include 3 types of black poly-paramagnetic polyethylene microspheres (range of diameters: 90-106 $\mu\text{m}$ ; 180-212 $\mu\text{m}$ ; and 250-300 $\mu\text{m}$ , respectively) and one type of clear paramagnetic polyethylene microsphere (180-212 $\mu\text{m}$ ). The black and clear particles with the same size range (180-212 $\mu\text{m}$ ) help to observe the influence of scattering on the measurement. The microspheres are supplied into the

measurement volume using a mini-funnel with a 1mm ID nozzle, in which the initial velocity of particles at the funnel nozzle exit is zero and the gravity velocity can be estimated using the distance from the nozzle exit. Two mono-dispersed drop streams generated using two medical syringes with ID=210 and 410  $\mu\text{m}$  respectively, are also used in this test. Low volume flow-rates (5 and 10 mL/min for the 210 $\mu\text{m}$  ID and 410 $\mu\text{m}$  ID syringe, respectively) result in Rayleigh breakup regimes, such that the droplet diameter is approximately equal to  $1.89 \times \text{ID}$  [12]. The velocity of liquid drops can also be estimated using the nozzle velocity with an account for spray-momentum decay due to drag [13]. The gravity velocity of microspheres and liquid drops are used as references for determining uncertainty in the measurement. The diameters range from 100-300  $\mu\text{m}$  for the microspheres and 400-800 $\mu\text{m}$  for the syringe-generated drops.

An in-house image processing script, which has been developed using a Matlab package and utilized previously in [10], is extended here to process two viewing-planes oriented 90 degrees to each other with PIV modes applied for both planes. This image processing code is used to process the two-angle double exposure images from the mono-dispersed drop streams generated from two syringes described earlier along with the poly-microsphere streams created from the mini-funnel. In this contribution, the liquid droplets will be called “drops” while “particles” or “microspheres” refer to the poly- polyethylene microspheres.

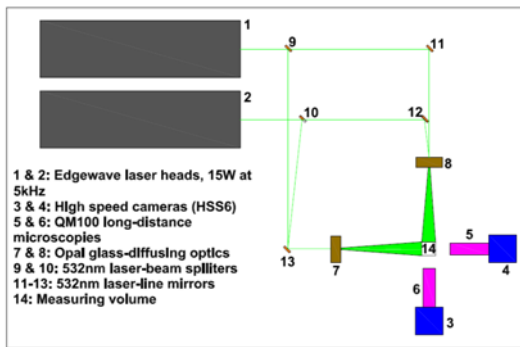


Figure 1. Schematic of experiment setup

Figure 2 illustrates the backlit shadows of one drop. Four 2D-images appear in frames (a) to (d) and indicate 2xdouble-angle images of the drop at two different times under a PIV mode of operation. Images shown in Figure 2a and 2c are taken at the initial time,  $t_0$ , by camera 1 and camera 2, respectively; similarly for shadows shown in Figure 2b and 2d, but at time  $t_1$  (the delay time used in the PIV setup,  $dt=t_1-t_0$ ). The shadows are binarized as described in [10] and their boundaries are used to generate 4 corresponding 2D-ellipses (the red ellipses shown in Figures 2a to 2d) using the least-square fitting approach. Each pair of ellipses generated from the two frames at the same time (pair 1: ellipses in frame (a) and frame (c); pair 2: ellipses in frame (b) and frame (d)) is used to generate a 3D-ellipsoid, and the two resulting 3D ellipsoids are shown in frames (e) and (f), which contain volume and velocity information of the drop. A 3D-ellipsoid is generated from the two 2D-ellipses by using the major and minor axes of the 2D images and the relevant rotation angles. The equivalent axis length of the 3D-ellipsoid is then determined based on the computed dimensions and rotations measured in two viewing planes. The full approach for volume reconstruction is shown elsewhere [11] and has yielded an uncertainty of the order of 10%. The velocity of the drop can be estimated through tracking the locations of the 3D ellipsoids at times  $t_0$  and  $t_1$  thereby strictly making this technique a particle tracking velocimetry (PTV) method. As mentioned, only results for velocity measurements will be reported here, details for the construction of a 3D ellipsoid from 2D ellipses is presented elsewhere [11]. For velocity

measurement, we consider a 3D ellipsoid with centroid coordinates  $(X,Y,Z)$  and 2D ellipses with coordinates  $(X_1,Y_1)$ , and  $(X_2,Y_2)$  from frames 1 and 2, respectively. In this work,  $X=X_1$ ;  $Y=X_2$ ; and  $Z=0.5(Y_1+Y_2)$ . Although the velocity can be expressed in three dimensions,  $(X, Y, Z)$ , only the vertical velocity ( $V_z$ ) will be reported here as the movement of the drops/particles in these experiments are mainly due to gravity. At time  $t_0$  and  $t_1$ , the centroids of two 3D ellipsoids will be  $(X_{t_0}, Y_{t_0}, Z_{t_0})$  and  $(X_{t_1}, Y_{t_1}, Z_{t_1})$ , respectively. The velocity  $V_z$  is therefore calculated simply as  $(Z_{t_1} - Z_{t_0})/(t_1-t_0)$ . Throughout this paper an ellipse refers to a 2D object generated from drop or particle boundaries while an “ellipsoid” refers to a 3D-object generated from the two 2D-ellipse frame images.

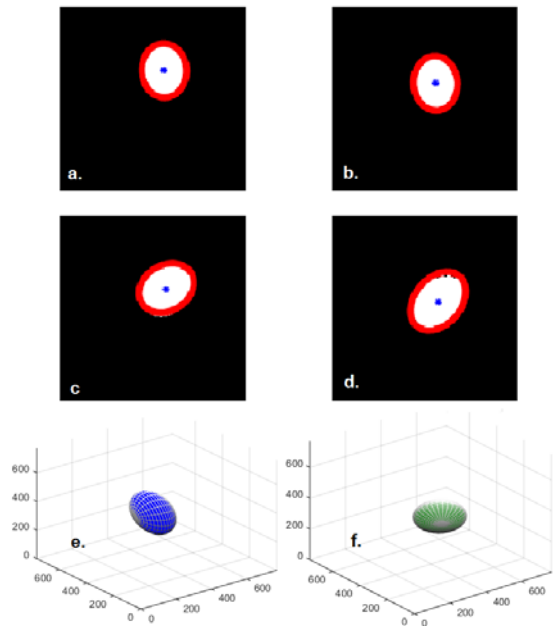


Figure 2. Description of ellipsoidal technique: a. camera 1 shot 1; b. camera 1 shot 2; c. camera 2 shot 1; d. camera 2 shot 2, time interval  $dt=40 \mu\text{s}$ ; e and f are the 3D-ellipsoids generated from the two 2D-ellipses imaged by two cameras at the same time,  $t_0$  and  $t_1$ , respectively.

It should be noted that for measuring the velocity of these falling droplets (which move slowly under gravity), double exposure is strictly not necessary and the time resolution of a single camera (in this case  $dt=200\mu\text{s}$ ) is sufficient here. Furthermore, as the drops/particles are almost spherical, similarity in velocity output information from a 2D boundary and that of a 3D ellipsoid can be expected. This is unlikely to be true for complex fragments however and therefore we examine both methods here for comparative purposes using spherical objects. Along with determining the particle/drop velocity using the centroid (of either a 2D boundary or 3D ellipsoid), other tracking locations include the top and bottom of the boundaries/ellipsoids. The top and bottom locations are defined as the maximum & minimum vertical axial values of the boundaries/ellipsoids, respectively. Velocities of those locations are very useful references for this measurement. Due to the similarity between velocity observed here for top and bottom locations, only velocity for the bottom location will be reported in this work. In summary, four different terminologies used in this report include the velocity of ellipsoid’s center, bottom, boundary center, and boundary bottom. Similarity in velocity of those locations could be expected for the spherical drops/particles and this will be examined in the following section.

## Results and Discussion

Boundary and ellipsoid velocity output for mono-dispersed drops is shown in Figure 3 versus the binary threshold value. The

nomenclature “binarized thresholding level” or “threshold level” used throughout this work is a normalization of the pixel intensity by the background intensity. As shown clearly in Figure 3, the velocity of ellipsoid and boundary center for drops generated from 210um ID syringes is identical to that of ellipsoid and boundary bottom. Here, the ellipsoid velocity is measured using the double exposure technique with  $dt=40\mu s$  (PIV mode) and the boundary velocities using single exposure ( $dt=200\mu s$  based on a 5Khz camera repetition rate). For the single exposure boundary velocities the velocity is taken as the average velocity measured from all frames. The velocity values remain almost constant in a range of thresholding level between 25-45%. This is also true for drops injected from 410 um ID syringe. The drops are almost spherical and therefore similarity in velocity output using the boundary or ellipsoid’s center or bottom is expected. It is notable that the ellipsoid velocity shown in Figure 3 is output from a dataset for an interval (double-exposure) time  $dt = 40 \mu s$  only, however, different time intervals ( $dt$  from 10 to 90  $\mu s$ ) have also been tested and the results are in excellent agreement to those plotted in this figure confirming the PTV code operation.

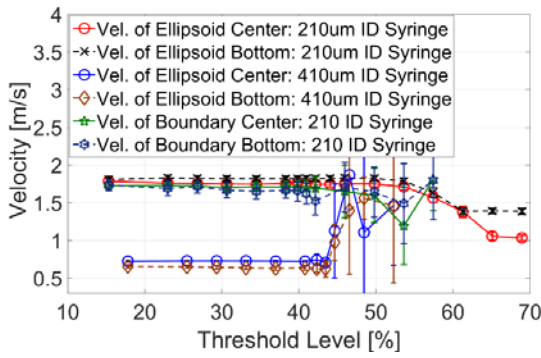


Figure 3. Mono-dispersed drop velocity with standard error bars estimated using the ellipsoidal technique (indicated as “ellipsoid”) with  $dt=40\mu s$  along with “boundary” center and bottom velocity. The estimation of velocity using boundaries of 2D-ellipses (indicated as “boundary” in the legends) are based on single exposure imaging with  $dt=200 \mu s$ .

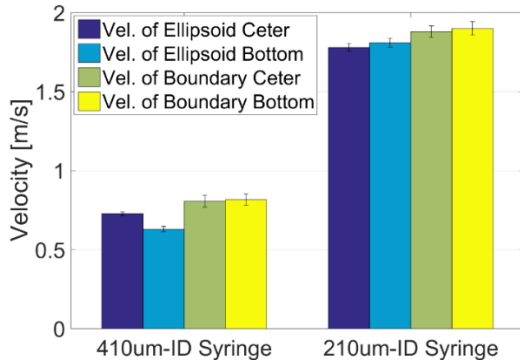


Figure 4. Mean velocity of mono-dispersed drops with standard error bars estimated from: (1) ellipsoid center; (2) Ellipsoid bottom; (3) drop boundary center and (4) drop boundary bottom. The binarised threshold level used here is 40%; the delay time applied for PIV measurement of the ellipsoid is  $dt=40\mu s$ . The estimation of velocity using boundaries of 2D-ellipses (indicated as “boundary” in the legends) are based on a single exposure  $dt=200 \mu s$ .

Mean boundary and ellipsoid velocities along with their corresponding standard-error bars are shown in Figure 4 with a binarized thresholding level of 40%. The standard error bars are estimated here with 95% of confidence using:  $error=1.96*\delta/n^{0.5}$ , where  $\delta$  is the standard deviation of a total of  $n$  samples. The theoretical velocity of the drops can be calculated from measuring the location and taking into account droplet deceleration from the nozzle exit due to drag [13]. The theoretical values are quite close to those reported in Figure 4.

Figure 5 shows the microsphere velocity measurement plotted versus binary threshold level. The velocity is almost constant in the threshold range between 25-45%, in excellent agreement with Fig. 3.

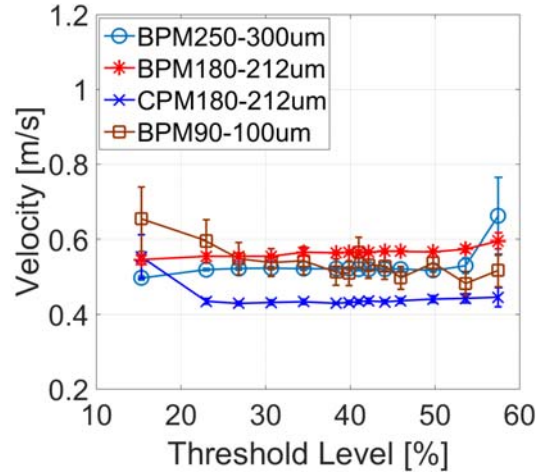


Figure 5. Solid particle center velocity with standard error bars estimated using the ellipsoidal technique, the values are for ellipsoid center; the delay time applied is  $dt=40\mu s$ . (‘B’ and ‘C’ in the legends stand for black and clear in colour of the particles, respectively; following the colour codes is the diameter range of the mono-dispersed particles).

The velocity of the black spheres are within close agreement whilst that of the clear counterparts is lower. There is no evidence for the effect of sphere size on the particle velocity, and here this is expected as the particles are falling due to gravity only. The lower velocity of the clear micro-polyspheres (C180-211um) requires further investigation.

Figure 6 shows the mean velocity of micro-polyspheres and standard error bars output with a thresholding level of 40%. As mentioned earlier, the particles are assumed to fall by gravity with a zero initial velocity from the funnel nozzle exit. As such, the gravity or theoretical velocity at a distance  $L$  from the funnel nozzle exit can be estimated using equation:  $v=v_0+g.t= v_0+\sqrt{2.g.L}$ , where  $v$  is particle velocity;  $v_0$  is initial velocity ( $v_0=0$  in this case);  $g$  is gravity; and  $L$  is distance from funnel nozzle exit to the middle of the measuring volume. With an approximate distance of 15 mm used in this experiment, it results in an average gravity velocity of 0.54 m/s and the gravity velocity is plotted in Figure 6 for reference (the solid horizontal line). It is clear from Figure 6 that the velocity measurements for those particles (both center and bottom) are within a deviation of about  $\pm 15\%$  from the theoretical value. It is notable here that the velocity estimated due to the acceleration of gravity when the particles enter the measuring volume ( $L\sim 13.75$  mm) is 0.52 m/s and then exit at 0.56 m/s ( $L\sim 16.25$  mm). The velocity shown in Figure 6 is in excellent agreement with this range (0.52-0.56 m/s).

A further issue that needs to be addressed, due to binarization of the images is the focused/defocused degree of the droplets. An approach to address this issue is to correlate drop size and velocity with a known defocusing distance. This issue has been addressed carefully for fragment sizes as well as size distribution when using a single-frame technique [9-10]. An extension is needed here to include the effect of defocusing level on volume and velocity using the double-frame technique in PIV mode. The drops are used for this purpose and are kept focused on one camera (camera 1 in this case) while incrementally defocused in the other camera, in a similar approach used in [10]. Figure 7 shows the velocity of mono-dispersed drops, injected by the 210um ID syringe, versus binary threshold level. Spray “foc1” refers to drops focused at both cameras; while the defocused level varies from “foc2” to

“foc6”, “foc6” is the most defocused. The defocused distances used here are 0; 0.61; 1.08; 1.17; 1.57 and 1.80 mm for spray “foc1” to “foc6”, respectively. These are the relative horizontal positions of drops with respect to that of focused spray “foc1” and calculated as the difference between the average of drops’ horizontal coordinates,  $X$ , and that of spray “foc1”.

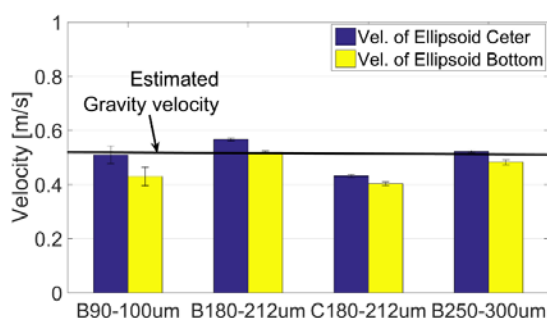


Figure 6. Mean of solid particle velocity with standard error bars estimated from: (1) ellipsoid center and (2) Ellipsoid bottom. The binary threshold level used here is 40%; the delay time is  $dt=40\mu s$ . ('B' and 'C' in the x-axis label stand for black and clear in colour of the particles, respectively; following the colour codes is the diameter range of the mono-dispersed particles).

As shown clearly in Figure 7, the defocusing level does affect the velocity output, with more defocusing leading to a lower measured velocity. A factor can be applied to correct this variation, which might be estimated for each fragment using the normalization of sum of light intensity passed through the fragment by its binarized area and this will be subject to future study. As shown in Figure 7, without correcting, a variation of 15% in velocity of those sprays is obtained when a thresholding level of 40% is applied.

## Conclusions

This work reports on the feasibility of velocity measurements based on an in-house coded PTV method for sprays using a double-frame imaging technique which can also be applied for simultaneous volume/velocity measurement of any object shape. An extensive error analysis is performed for mono-dispersed drops as well as poly-microsphere streams. The drops are generated using a medical syringe pump while the microsphere streams are created using a well-designed mini-funnel (1mm diameter). The microsphere diameters range from 100 to 300  $\mu m$  while the drop diameter ranges from 400 to 900  $\mu m$ . Measurements are compared to theoretical droplet and particle velocity calculations. Velocities of different points of a given droplet (center & bottom) from boundary of the 2D shadows as well as 3D ellipsoids are presented. Consistent results are obtained for different points (center and bottom) of the boundary/ellipsoids under different double-exposure time intervals (20 to 90  $\mu s$  used in this study). This confirms the technique can be applied to measure local velocities of a given object at different points along its surface (to measure oscillation velocity of ligaments for instance).

The velocity of 3D ellipsoids output using the ellipsoidal technique is also compared against that output using boundaries of drops and microspheres obtained from the 2D image frames. The velocity values are found to remain almost constant when using thresholding levels between 25-45%. Without a correction for the defocusing issue, a deviation of approximately 15% is observed between the most defocused spray to the focused counterpart at a thresholding level of 40%. At this thresholding level, a variation of 15% is observed when comparing the measured velocity with theoretical one. Future work shall include: (1) Examining the technique to measure volume combined with volume measurements; and (2) Applying the technique for real spray

measurements providing the first available measurements of combined velocity and volume of arbitrarily shaped fragments.

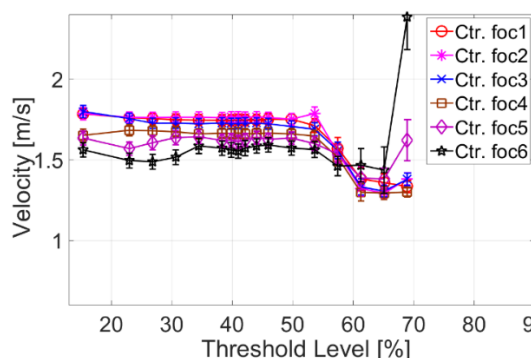


Figure 7. Velocity of mono-dispersed drops at different defocusing level versus thresholding level. (Scripts in the legends: “Ctr.” stands for centroid of the ellipsoid; spray “foc1” is focused at both cameras; while sprays “foc2” to “foc6” are at different defocusing levels applied to camera 1 while always remained focused in the other (camera 2), “foc6” is the most defocused)

## Acknowledgments

This paper was made possible by a NPRP award [NPRP 7-036-2-018] from the Qatar National Research Fund (a member of The Qatar Foundation). The statements made herein are solely the responsibility of the authors.

## References

- [1] C. M. Varga, J. C. Lashera, E. J. Hop\_nger, Initial breakup of a small diameter liquid jet by a high-speed gas stream, *J. Fluid Mech.* 497 (2003) 405-435.
- [2] C. Dumouchel, On the experimental investigation on primary atomization of liquid streams, *Experiments in Fluids* 45 (2008) 371-422.
- [3] L. P. Hsiang, G. M. Faeth, Near-limit drop deformation and secondary breakup, *Int. J. Multiphase Flow* 18(5) (1992) 35-652.
- [4] A. B. Liu, R. D. Reitz, Mechanism of air-assisted liquid atomization, *Atomization and Sprays* 3 (1993) 55-75.
- [5] S. Ghaemi, P. Rahimi, D. S. Nobes, Assessment of parameter for distinguishing droplet shape in a spray field using image-based technique, *Atomization and Sprays* 19(9) (2009) 809-831.
- [6] A. Masri, *Turbulent Combustion of Sprays: from Dilute to Dense*, accepted in *Combustion Science and Technology*, 2016
- [7] P. Pham, T. Bodisco, S. Stevanovic, M. Rahman, H. Wang, Z. Ristovski, R. Brown, A. Masri, Engine performance characteristics for biodiesels of different degrees of saturation and carbon chain lengths, *SAE Int. J. of Fuels and Lubricant* 6(1) (2013) 188-198.
- [8] P. X. Pham, T. A. Bodisco, Z. D. Ristovski, R. J. Brown, A. R. Masri, The influence of fatty acid methyl ester profiles on inter-cycle variability in a heavy duty compression ignition engine, *Fuel* 116 (2014) 140-150.
- [9] A. Kourmatzis, P. X. Pham, A. R. Masri, Air assisted atomization and spray density characterization of ethanol and a range of biodiesels, *Fuel* 108 (2013) 758-770.
- [10] A. Kourmatzis, P. X. Pham, A. Masri, A burner for the characterization of atomization and combustion characteristics in turbulent spray flames, *Combustion and Flame* 162 (4), (2014) 978-996
- [11] A. Kourmatzis, P.X. Pham, A.R. Masri, A two-angle far-field microscope technique for spray flows, Submitted, 2016
- [12] A. H. Lefebvre, *Atomization and Sprays*, Taylor & Francis, 1988.
- [13] H. Lienemann, *Momentum Coupling in Transient Multiphase Flows*, PhD Thesis, Imperial College London, 2004.